X-ray Absorption Studies of the Ferrous Active Site of Isopenicillin N Synthase and Related Model Complexes†

Clayton R. Randall, Yan Zang, Anne E. True, and Lawrence Que, Jr.*

Department of Chemistry, University of Minnesota, Minneapolis, Minnesota 55455

John M. Charnock and C. David Garner*

Department of Chemistry, University of Manchester, Manchester M13 9PL, U.K.

Yoshiyuki Fujishima, Christopher J. Schofield, and Jack E. Baldwin*

The Dyson Perrins Laboratory, Oxford University, Oxford OX1 3QY, U.K.

Received December 15, 1992; Revised Manuscript Received April 12, 1993

ABSTRACT: Isopenicillin N synthase (IPNS) from *Cephalosporium acremonium* (M_r 38 400) is an iron-containing enzyme that aerobically catalyzes the four-electron oxidative ring closure reactions of δ-(L-α-aminoadipoyl)-L-cysteinyl-D-valine (ACV), forming the β-lactam and thiazolidine rings of isopenicillin N. Here, we report Fe K-edge X-ray absorption studies that provide insight into the iron coordination environment and the effect of substrate and nitric oxide binding. Our analysis reveals an iron(II) coordination environment consisting of two N/O-containing ligands at 2.01 ± 0.02 Å, three N/O ligands at 2.15 ± 0.02 Å, and one C/O scatterer at approximately 2.6–2.7 Å. Three His ligands are associated with the 2.15-Å shell, while an unsymmetrically chelated carboxylate is associated with a scatterer at 2.01 and at 2.6–2.7 Å, a combination which is consistent with the ligand environment deduced from ^{1}H NMR studies [Ming, L.-J., Que, L., Jr., Kriauciunas, A., Frolik, C. A., & Chen, V. J. (1991) *Biochemistry 30,* 11653–11659]. The remaining scatterer at 2.01 Å is assigned to a coordinated solvent molecule, most likely hydroxide, which can act as the proton acceptor for the incoming substrate. ACV binding to Fe(II)IPNS evinces an Fe–S interaction at 2.35 ± 0.02 Å, indicative of the coordination of substrate cysteine thiolate to the metal center. Analysis of the Fe(II)IPNS–ACV–NO data reveals one Fe–N at 1.71 ± 0.02 Å, three Fe–(N,O) at 2.04 ± 0.02 Å, one Fe–S at 2.32 ± 0.02 Å, and one Fe–(C,O) at 2.61 ± 0.02 Å, the short Fe–N bond being derived from the binding of NO. Our EXAFS conclusions, supported by corresponding analysis of relevant model complexes, corroborate and refine the working model for the Fe(II) coordination environment developed from previous spectroscopic studies.

The key steps in the biosynthesis of penicillin- and cephalosporin-related antibiotics in some microorganisms are the oxidative ring closure reactions of δ-(L-α-aminoadipoyl)-L-cysteinyl-D-valine (ACV),[1] forming the β-lactam and thiazolidine rings of isopenicillin N, the precursor of other

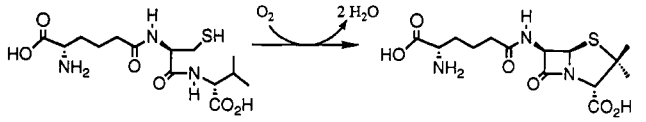

ACV Isopenicillin N

penicillins and cephalosporins (Baldwin & Bradley, 1990; Baldwin, 1988; Baldwin & Abraham, 1988; Robinson, 1988). The enzyme isopenicillin N synthase (IPNS) aerobically catalyzes this four-electron oxidative process and contains a single high-spin non-heme iron(II) center in its active site (Chen *et al.*, 1989a,b). However, unlike in the oxidative ring cleavage reactions catalyzed by non-heme iron-containing catechol dioxygenases in which the oxygen atoms are incorporated into the substrates (Que, 1989), dioxygen is completely reduced to 2 equiv of water in the oxidative ring closure reactions of ACV by IPNS.

The mechanism of catalysis by IPNS has been extensively studied by the use of many different substrate analogues (Baldwin & Bradley, 1990; Baldwin, 1988; Baldwin & Abraham, 1988; Robinson, 1988); however, details of the coordination environment of the active site iron atom are only just beginning to emerge. EPR, ^{57}Fe Mössbauer, electronic, and NMR spectroscopic studies have been conducted on Fe(II)IPNS and on its cobalt(II) and copper(II) derivatives, Co(II)IPNS and Cu(II)IPNS (Chen *et al.*, 1989a,b; Jiang *et al.*, 1991; Ming *et al.*, 1990). Combined, these studies have resulted in the proposal that the metal is bound by three endogenous histidine ligands, leaving three available sites for exogenous ligands such as solvent, substrate Cys–S$^-$, and dioxygen or NO. Recently, this model was refined on the basis of NOE studies to include a carboxylate moiety, probably from aspartate, as a fourth endogenous ligand (Ming *et al.*, 1991).

† XAS studies at the University of Minnesota are supported by the NIH (GM 33162). XAS studies at the University of Manchester are supported by the SERC. Work performed at Oxford University is supported by the SERC and Eli Lilly and Co. C.D.G. is grateful to the Director of the Daresbury Laboratory for the provision of facilities. C.R.R. gratefully acknowledges a traineeship from the U.S. Public Health Service (GM 07323). Beamline X9 at the NSLS at BNL is supported by the NIH (RR-001633), while CHESS is supported by the NSF (DMR-8412465).

* Author to whom correspondence should be addressed.

[1] Abbreviations: ACV, δ-(L-α-aminoadipoyl)-L-cysteinyl-D-valine; EXAFS, extended X-ray absorption fine structure; IPNS, isopenicillin N synthase; HB(^{i}Pr$_2$pz)$_3^-$, hydrotris(3,5-diisopropylpyrazol-1-yl)borate(−1); TLA, tris(6-methyl-2-pyridylmethyl)amine; TMPzA, tris(3,5-dimethylpyrazol-1-ylmethyl)amine; TPA, tris(2-pyridylmethyl)amine; XANES, X-ray absorption near-edge spectroscopy.

0006-2960/93/0432-6664$04.00/0

In this paper, we use Fe K-edge X-ray absorption studies on IPNS samples and relevant model complexes to support the refined spectroscopic model and provide further insight into the effect of substrate and nitric oxide binding on the coordination environment of Fe(II)IPNS. In particular, we provide evidence for an endogenous carboxylate ligand and show that the substrate ACV is bound by its cysteinyl sulfur atom to the active site iron in both the Fe(II)IPNS–ACV and Fe(II)IPNS–ACV–NO complexes.

EXPERIMENTAL PROCEDURES

Preparation of Protein Samples and Model Complexes. Cephalosporium acremonium isopenicillin N synthase (MW 38 400) was purified as the apoprotein from recombinant *Escherichia coli* according to published procedures (Kriauciunas *et al.*, 1991; Baldwin *et al.*, 1990) and stored in 0.1 M MOPS buffer at pH 7.1 in liquid nitrogen. The substrate ACV is a product of Incell (Milwaukee, WI), nitric oxide is from Matheson (Secaucus, NJ), and all other reagents used were of the highest grade available commercially. Fe(II)IPNS activity was determined by the initial rate of consumption of dioxygen by a solution of Fe^{II}–reconstituted enzyme in the presence of 5 mM ACV and ascorbate in 0.1 M MOPS buffer at pH 7.1. Oxygen consumption was monitored by an oxygen-sensitive electrode; alternatively, the activity can be estimated by the direct measurement of isopenicillin N produced under the above conditions using HPLC (Kriauciunas *et al.*, 1991). Those preparations with a high specific Fe(II)IPNS activity of 4–7 units/mg were used in this study [1 unit of Fe(II)IPNS activity is defined as 1 μmol of O_2 consumed/min under the conditions described above at 25 °C]. These specific activity values are comparable to those of samples used in previous spectroscopic investigations. The Fe^{II}–reconstituted enzyme was prepared by direct infusion of 1 equiv of metal ion into the apoprotein in 0.1 M MOPS buffer at pH 7.1. All samples were prepared under an anaerobic atmosphere which was achieved by repeated cycles of evacuation and flushing with argon that had been passed at 170 °C over a column of copper catalyst (Chemical Dynamics, South Plainfield, NJ) to remove residual oxygen. Fe(II)IPNS–ACV was prepared by the anaerobic addition of ACV in 0.1 M MOPS buffer at pH 7.1 to a sample of Fe(II)IPNS, producing a solution approximately 90 mM in ACV, which is 5 times the K_d for the dissociation of ACV from the enzyme–substrate complex, as measured by Mössbauer spectroscopy (Orville *et al.*, 1992). Fe(II)IPNS–ACV–NO was prepared by directly bubbling nitric oxide gas that had been passed through a saturated solution of NaOH into a sample of Fe(II)IPNS–ACV using a gastight syringe (Hamilton, Reno, NV). All protein samples used were approximately 3–4 mM in Fe^{II}.

The synthesis and characterization of [(HB(^{i}Pr$_2$pz)$_3$)Fe(OBz)] has already been described (Kitajima *et al.*, 1990). The syntheses and characterization of [(TPA)Fe(S-2,4,6-$Me_3C_6H_2$)](ClO_4) and [(TMPzA)Fe(NO)Cl](BPh_4) will be described in subsequent papers.

EXAFS Data Collection and Analysis (U.S.). X-ray absorption spectra (XAS) were collected between 6.9 and 8.1 keV at station C2 of the Cornell High Energy Synchrotron Source (CHESS) and at beamline X9 of the National Synchrotron Light Source (NSLS) at Brookhaven National Laboratory. The monochromator was calibrated by using the 1s → 3d feature at 7113.0 eV in the XAS spectrum of (NEt_4)[$FeCl_4$]. The XAS data for the model complexes were obtained in transmission mode ($A_{exp} = -\log_{10} I_t/I_0$) as dispersions of the microcrystalline solids in boron nitride at room temperature. The XAS data for the Fe(II)IPNS samples were obtained in fluorescence mode at 77 K. A_{exp} (C_f/C_0) was determined from an incident (C_0) ionization detector and a final fluorescence (C_f) detector. A large solid-angle Lytle fluorescence detector was used with an Mn filter and Soller slits (Stern & Heald, 1979).

The treatment of the raw EXAFS data to yield X is discussed at length in several review papers (Teo, 1981; Scott, 1985). Details of our data treatment procedure, including correction of fluorescence data for thickness effects and detector response, have been presented previously (Scarrow *et al.*, 1987). The refinements reported were of RMS_{dev}/RMS_{dat} of k^3X data, and the function minimized was $R \equiv [\sum k^6(X_c - X)^2/n]^{1/2}$, where the sum is over n data points between 2 and 14 Å^{-1} [2–12 Å^{-1} for Fe(II)IPNS] (Scarrow *et al.*, 1987).

Single-scattering EXAFS theory allows each shell of n scatterers to be modeled separately, with the EXAFS spectrum described as a sum of each shell (Scarrow *et al.*, 1987)

$$X_c = \sum_{\text{shells}} nA[f(k)k^{-1}r^{-2}\exp(-2\sigma^2k^2)\sin[2kr + \alpha(k)]]$$

where $k = [8\pi^2m_e(E - E_0 + \Delta E)/h^2]^{1/2}$. The amplitude reduction factor (A) and the shell-specific edge shift (ΔE) are empirical parameters that partially compensate for imperfections in the theoretical amplitude and phase functions f and α (Teo & Lee, 1979).

The analysis procedure, a variation of FABM ("fine adjustment based on models") (Teo *et al.*, 1983), uses theoretical phase and amplitude functions. For each shell, crystallographically characterized model complexes such as [$Fe(acac)_3$] are used to determine A and ΔE (Teo & Lee, 1979). The amplitude reduction factor and edge shift used for ligand O/N atoms were 0.43 and 3 eV, respectively. Those used for more distant O/C atoms in the first coordination sphere, as well as for outer coordination sphere N/C atoms, were 0.38 and −3 eV, respectively. A and ΔE for S and Cl atoms were 0.40 and −1 eV and 0.39 and 6 eV, respectively. This leaves two parameters per shell (r and n or σ^2) to be refined instead of the four parameters refined using BFBT ("best fit based on theory") (Teo *et al.*, 1983).

Recent studies have indicated that the single-scattering EXAFS theory is valid to lower energies than previously believed (Bunker & Stern, 1984; Müller & Schaich, 1983). However, the amplitude and phase function tables of Teo and Lee (1979) were calculated using a plane wave approximation for the scattering of the photoelectron wave by the neighboring atom and are unsatisfactory at low photoelectron momentum. Recently, McKale *et al.* (1988) have calculated amplitude and phase shift functions for $2 \le k \le 20$ Å^{-1} using a spherical wave formalism, thus extending the range of EXAFS data that can be used in refinement to $k = 2$ Å^{-1}. Use of these "curved-wave" functions has consistently yielded better fits than those determined with the Teo–Lee tables, although using data at low photoelectron momentum raises the question of whether other effects such as XANES may be contributing to the EXAFS spectrum. However, in both model compounds and proteins, analysis of the data in the range $2 \le k \le 14$ Å^{-1} gave identical fits to those using data in the range $3 \le k \le 14$ or even $4 \le k \le 14$. Thus, it can be assumed that contributions from phenomena other than EXAFS are negligible in the k range ($2 \le k \le 14$ Å^{-1}) used in the fits presented here [$2 \le k \le 12$ Å^{-1} for Fe(II)IPNS].

EXAFS Data Collection and Analysis (U.K.). X-ray absorption data for Fe(II)IPNS were recorded on station 8.1 of the Daresbury SRS operating at 2 GeV and an average

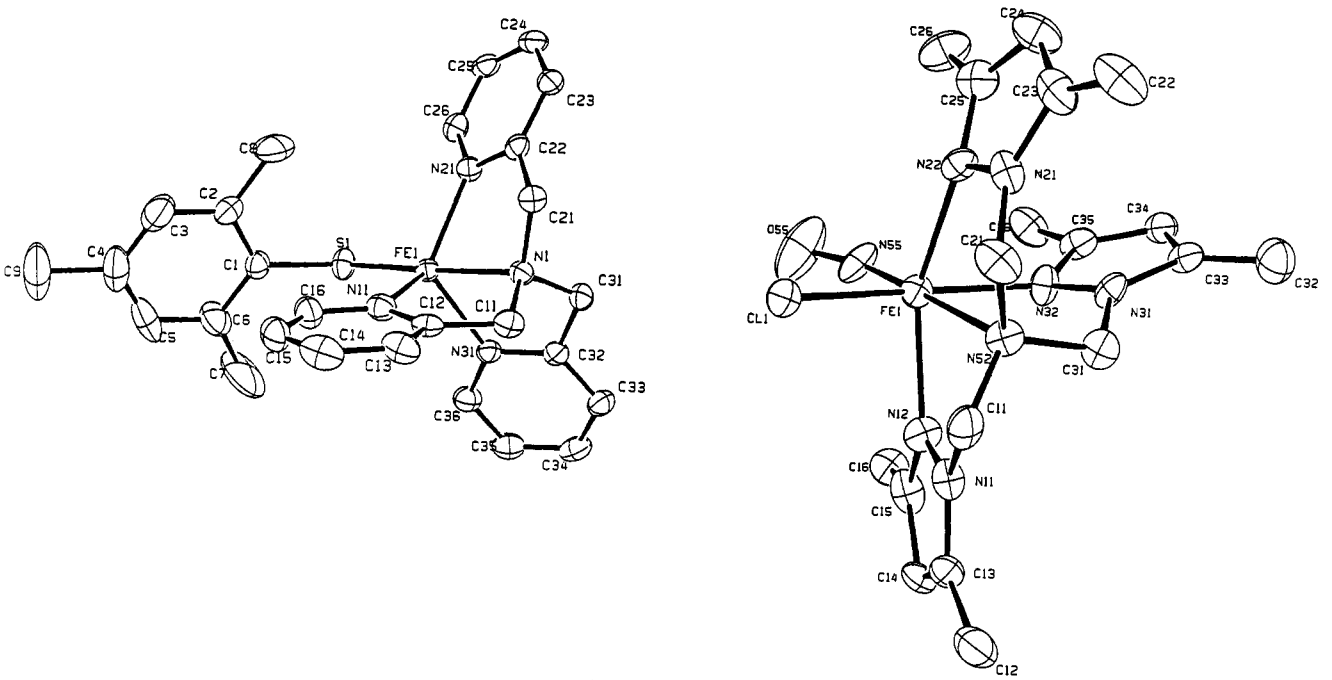

FIGURE 1: (a, left) ORTEP plot of the crystal structure of the $[(TPA)Fe(S\text{-}2,4,6\text{-}Me_3C_6H_2)]^+$ cation. Selected bond lengths (Å) and angles (deg) are as follows: Fe–S, 2.345 (1); Fe–N1, 2.250 (3); Fe–N11, 2.135 (4); Fe–N21, 2.119 (3); Fe–N31, 2.123 (3); S–C1, 1.774 (4); S–Fe–N1, 173.8 (1); S–Fe–N11, 110.2 (1); S–Fe–N21, 100.6 (1); S–Fe–N31, 101.8 (1); Fe–S–C1, 113.5 (2). (b, right) ORTEP plot of the crystal structure of the $[(TMPzA)Fe(NO)Cl]^+$ cation. Selected bond lengths (Å) and angles (deg) are as follows: Fe–Cl, 2.335 (3); Fe–N12, 2.160 (9); Fe–N22, 2.170 (9); Fe–N32, 2.140 (9); Fe–N52, 2.287 (6); Fe–N55, 1.735 (7); N55–O55, 1.15 (1); Cl–Fe–N12, 90.4 (2); Cl–Fe–N22, 91.6 (2); Cl–Fe–N32, 167.2 (2); Cl–Fe–N52, 89.8 (2), Cl–Fe–N55, 91.6 (3); Fe–N55–O55, 157.1 (8).

current of 200 mA, using a Si(111) focusing monochromator and a Canberra 13-element fluorescence detector. Scans were recorded for a *ca.* 1 mM solution of IPNS plus Fe^{II} in 20 mM Tris-HCl buffer at pH 8.0 that was frozen and maintained at 77 K. The isolated EXAFS data were analyzed over the range $2.5 \leq k \leq 15$ Å^{-1} using EXCURV92 (Binsted *et al.*, 1991), employing the single scattering, spherical wave approximations described above with phase shifts derived from *ab initio* calculations using Hedin–Lundqvist potentials (Lee & Pendry, 1975; Gurman *et al.*, 1984; Hedin & Lundqvist, 1969). Addition of multiple scattering (Gurman *et al.*, 1986) from the outer shells of the imidazole groups did not lead to any significant improvement of the fits and so was not included in the final analysis.

Integration of the 1s → 3d Peak. The pre-edge areas were calculated by subtracting an arctangent function from the data and normalizing with respect to the edge jump height. The background function was determined by a least-squares fit of an arctangent together with a first-order polynomial to the data below the inflection point as previously described (Roe *et al.*, 1984). The area of the pre-edge peak after the background subtraction was obtained by integrating over a range of ~8 eV. This range centered on the peak, and any residual background function was interpolated over that range (Roe *et al.*, 1984). The edge jump was determined by fitting first-order polynomials to the data as previously described. The difference between these two lines at the inflection point of the edge was used as the normalization factor for the pre-edge peak area. For example, Fe(II)IPNS from *C. acremonium* has a normalized pre-edge area of 7.6×10^{-2} eV, which is abbreviated as 7.6 units.

RESULTS

Models for IPNS Species. X-ray absorption data were obtained for several iron(II) complexes that may serve as models for Fe(II)IPNS, Fe(II)IPNS–ACV, and Fe(II)IPNS–ACV–NO; they possess structural features expected to be present in the three IPNS species studied. The iron center of $(HB(^iPr_2pz)_3)Fe(OBz)$ is coordinated by three aromatic nitrogen ligands and one chelated carboxylate ligand, while that of $[(TPA)Fe(S\text{-}2,4,6\text{-}Me_3C_6H_2)](ClO_4)$ has three aromatic nitrogen ligands, an amine nitrogen ligand, and one sterically bulky thiolate ligand. The iron(II) center of $[(TMPzA)Fe(NO)(Cl)](BPh_4)$ contains three aromatic nitrogen ligands, an amine nitrogen ligand, a nitrosyl ligand, and a chloride ligand that has photoelectron scattering properties similar to those of sulfur. The structures of the latter two complexes are shown in Figure 1.

The Fe K-edge energies of both $(HB(^iPr_2pz)_3)Fe(OBz)$ and $[(TPA)Fe(S\text{-}2,4,6\text{-}Me_3C_6H_2)](ClO_4)$ are at approximately 7121 eV, which is consistent with the presence of Fe^{II} (Figure 2a). The absorption edge of $[(TPA)Fe(S\text{-}2,4,6\text{-}Me_3C_6H_2)](ClO_4)$ shows more of a tail at lower energy (below 7120 eV) than that of $(HB(^iPr_2pz)_3)Fe(OBz)$, reflecting the presence of the electron-donating arenethiolate ligand. The absorption edge of $[(TMPzA)Fe(NO)Cl](BPh_4)$ is at a higher energy (~7123 eV) than those of the other species studied, consistent with the more "ferric" character of the iron atom induced by nitric oxide binding. Our observation agrees with recent conclusions reached by Zhang *et al.* (1992) on other $\{Fe\text{–}NO\}^7$ complexes.

The pre-edge spectra of all three model complexes show features at approximately 7112 eV that can be assigned to the iron 1s → 3d transition (Shulman *et al.*, 1976). Previous studies of model compounds and molecular orbital calculations indicate that the intensity of these pre-edge features relative to the K-edge absorption intensity can be correlated with the amount of iron 4p and 3d orbital mixing and therefore with the coordination geometry around the iron atom. The pre-edge intensity generally increases with a decrease in coordination number and departure from a centrosymmetric coordination environment, *i.e.*, $I_{tetrahedral} > I_{5\text{-coord}} > I_{octahedral}$

Table I: Comparison of EXAFS Fits with Crystallographic Data of Model Complexes for IPNS Species

model[a]	n	Fe–N/O	n	Fe–N/O	n	Fe–N/O	n	Fe–S/Cl	n	Fe–C/O
$(HB(^iPr_2pz)_3)Fe(OBz)$										
EXAFS			4	2.09 (σ^2 = 0.004)					1	2.47 (σ^2 = 0.001)
crystal[b]			4	2.08	1	2.23			1	2.48
$[(TPA)Fe(S\text{-}Me_3C_6H_2)](ClO_4)$										
EXAFS			3	2.11 (σ^2 = 0.004)			1	2.33 (σ^2 = 0.001)		
crystal			3	2.13	1	2.25	1	2.34		
$[(TMPzA)Fe(NO)(Cl)](BPh_4)$										
EXAFS	1	1.75 (σ^2 = 0.002)	3	2.16 (σ^2 = 0.003)			1	2.38 (σ^2 = 0.005)		
crystal	1	1.74	3	2.16	1	2.29	1	2.34		

[a] Distances are in Å, and Debye–Waller factors (σ^2) are in Å^2. [b] The crystallographic information is from the structure of $(HB(3,5\text{-}^iPr_2pz)_3)Fe(OAc)$.

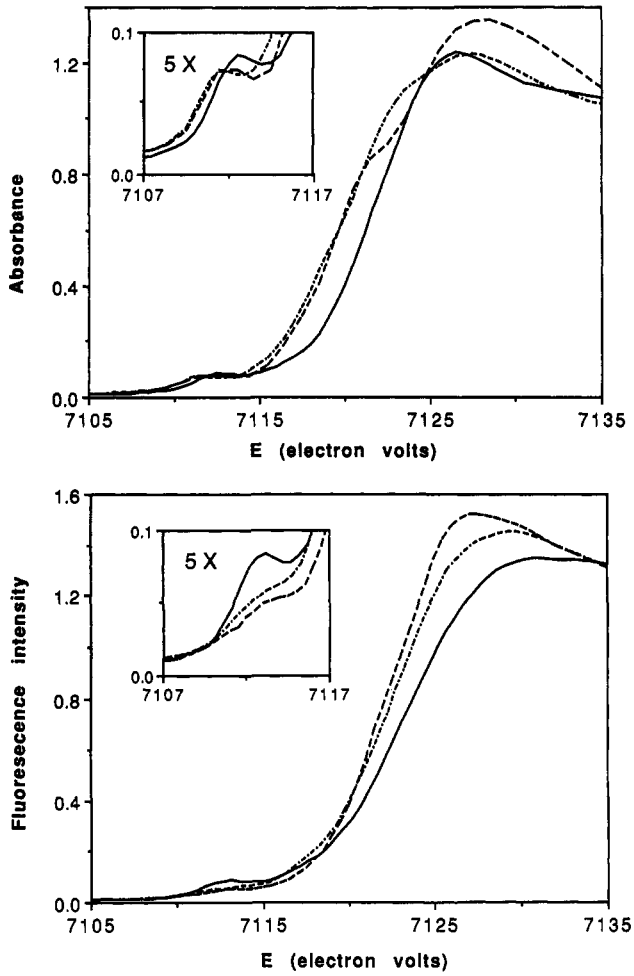

FIGURE 2: Pre-edge and XANES spectra. (a, top) Models for IPNS species: LFe(OBz) (- - -), $[(TPA)Fe(S\text{-}2,4,6\text{-}Me_3C_6H_2)](ClO_4)$ (- · -), and $[(TMPzA)Fe(NO)Cl](BPh_4)$ (—), with the 1s → 3d pre-edge features highlighted in the inset. (b, bottom) IPNS species: Fe(II)IPNS (- - -), Fe(II)IPNS–ACV (- · -), and Fe(II)IPNS–ACV–NO (—), with the 1s → 3d pre-edge features highlighted in the inset.

(Roe *et al.*, 1984). The 1s → 3d pre-edge peak areas of $(HB(^iPr_2pz)_3)Fe(OBz)$, $[(TPA)Fe(S\text{-}2,4,6\text{-}Me_3C_6H_2)](ClO_4)$, and $[(TMPzA)Fe(NO)Cl](BPh_4)$ were 10.7, 8.9, and 11.4 units, respectively.

$(HB(^iPr_2pz)_3)Fe(OBz)$ was chosen for study by X-ray absorption spectroscopy as a model for the active site of Fe(II)IPNS, and not its crystallographically characterized acetonitrile solvate, $(HB(^iPr_2pz)_3)Fe(OBz)(MeCN)$ (Kitajima *et al.*, 1990), because the latter exhibited spectra that varied in each of the four samples studied, probably due to some solvent loss upon irradiation. The area of the pre-edge feature observed for $(HB(^iPr_2pz)_3)Fe(OBz)$ (10.7 units) is consistent with five-coordination, as found for its recently crystallized acetate analogue $(HB(^iPr_2pz)_3)Fe(OAc)$.[2] The first shell contribution to the EXAFS of $(HB(^iPr_2pz)_3)Fe(OBz)$ can be modeled well with four Fe–N/O at 2.09 Å and one Fe–C/O at 2.47 Å. These values correspond to the first coordination sphere of $(HB(^iPr_2pz)_3)Fe(OAc)$, for which the average crystallographic Fe–N/O distance found for four of the ligands, three pyrazole nitrogens and one carboxylate oxygen, was 2.08 Å. In $(HB(^iPr_2pz)_3)Fe(OAc)$, the other carboxylate oxygen and the carboxylate carbon are, respectively, 2.23 and 2.48 Å from the Fe^{II} center. For $(HB(^iPr_2pz)_3)Fe(OBz)$, inclusion of backscattering from the more distant carboxylate oxygen atom at 2.23 Å did not improve the residual; however, the addition of the Fe–C/O interaction at 2.47 Å did so significantly. The residual of the multishell fit was 21% without the 2.47 Å interaction and 12% with it (Table I). A possible explanation for the failure to observe the carboxylate oxygen at 2.23 Å in the EXAFS is that the motion of this atom is not strongly correlated with that of the metal and, in this respect, it is noted that any change in the Fe–O distance will lead to a significantly smaller change in the $Fe\text{–}C_{carboxylate}$ distance.

The 1s → 3d pre-edge peak area of 8.9 units for $[(TPA)Fe(S\text{-}2,4,6\text{-}Me_3C_6H_2)](ClO_4)$ represents the lower end of the range for the five-coordinate iron complexes characterized so far but is still larger than the areas of most six-coordinate complexes (Roe *et al.*, 1984). However, the database upon which these ranges are based consists mainly of Fe(III) complexes, so the range of values for five-coordinate complexes may shift to lower values when only Fe(II) complexes are considered. At present, the number of Fe(II) complexes in the database is insufficiently large to allow these ranges to be defined. The Fe–L distances obtained from the EXAFS data are very similar to those obtained crystallographically. The EXAFS data were fit satisfactorily with three Fe–N at 2.11 Å and one Fe–S at 2.33 Å, with a residual of 14%; for comparison, the pyridine nitrogen atoms are at an average crystallographic distance of 2.13 Å, and the iron–sulfur distance is 2.34 Å (Figure 1a). The apical nitrogen atom at 2.25 Å is not required in the EXAFS simulations, probably due to the presence of a sulfur atom at a similar distance; the two backscattering contributions would be out of phase relative to each other with the sulfur wave dominant. Such a phenomenon has also been observed for zinc proteins having both nitrogen and sulfur ligation at similar distances (Garner & Feiters, 1987).

The pre-edge peak area of $[(TMPzA)Fe(NO)Cl](BPh_4)$ is unusually large for a six-coordinate "iron(II)" complex. This is most probably due to significant distortion from octahedral

[2] N. Kitajima, results to be published.

symmetry caused by the short Fe–$N_{nitrosyl}$ and results in enhanced metal 3d–4p mixing. The presence of short Fe–O_{oxo} bonds in oxo-bridged diferric complexes also gives rise to significantly higher 1s → 3d peak intensities than are usually observed for hexacoordinate iron(III) complexes for the same reason (Roe *et al.*, 1984). The EXAFS model has one short Fe–N interaction at 1.75 Å, three Fe–N interactions at 2.16 Å, and one Fe–Cl at 2.38 Å. This compares well to the crystal structure, which has an Fe–N at 1.74 Å, three Fe–N interactions at an average distance of 2.16 Å, and one Fe–Cl at 2.34 Å (Figure 1b). The tertiary amine nitrogen of the TMPzA ligand, which is *trans* to the nitrosyl ligand in the crystal structure and 2.29 Å from the iron atom, was not modeled in the fit, having a similar iron–ligand distance to that of the chlorine atom and the two backscattering contributions being out of phase with the chlorine dominant (*vide supra*). The residual of this fit was 9.2%.

The first coordination sphere distances obtained from fitting EXAFS data compared well with those obtained crystallographically for all three model complexes (Table I). Modeling of the outer coordination spheres did not produce any significant improvement of the fits and was therefore not included in the final data analysis.

IPNS Species. (a) Edge and Pre-Edge Spectra. The Fe K-edge energies of both Fe(II)IPNS and its enzyme–substrate complex are consistent with the presence of Fe^{II} (Figure 2b). The absorption edge of Fe(II)IPNS–ACV shows more of a tail at lower energy than that of Fe(II)IPNS, similar to that observed for [(TPA)Fe(S-2,4,6-$Me_3C_6H_2$)](ClO_4); this reflects the coordination of the ACV thiolate to the metal upon substrate binding. The absorption edge of the enzyme–substrate–nitric oxide complex [Fe(II)IPNS–ACV–NO] is at a higher energy than those of the other species studied, consistent with the corresponding results for the chemical systems and the observations of Zhang *et al.* (1992). ^{57}Fe Mössbauer studies of Fe(II)IPNS–ACV–NO also indicate that the iron is in an intermediate state between iron(II) and iron(III) (Chen *et al.*, 1989a; Orville *et al.*, 1992).

All three species show a pre-edge feature at approximately 7112–7113 eV that can be assigned to the iron 1s → 3d transition. For Fe(II)IPNS and Fe(II)IPNS–ACV, the 1s → 3d intensities are 7.6 and 8.1, respectively. Both values are lower than those of five-coordinate iron complexes but larger than those of most six-coordinate complexes (*vide supra*). Therefore, Fe(II)IPNS and Fe(II)IPNS–ACV have 1s → 3d peak areas consistent with either a five-coordinate or a distorted six-coordinate ligand environment. For Fe(II)IPNS–ACV–NO, the greater intensity of the pre-edge feature (13.1) reflects the coordination of nitric oxide to the enzyme–substrate complex (Figure 2b) and is similar to that of the six-coordinate model complex [(TMPzA)Fe(NO)(Cl)](BPh_4), which has a coordination environment similar to that which we propose for the enzyme–substrate–nitric oxide complex (*vide infra*).

(b) EXAFS Studies. It was possible to model the first coordination sphere of Fe(II)IPNS with one shell of five N/O scatterers at 2.09 Å (fit 1, Table II). However, this simulation had a large residual (RMS_{dev}/RMS_{dat}) of 22% and afforded a shell with a very large Debye–Waller factor (σ^2 = 0.011 Å^2), indicative of too large a range of metal–ligand distances among the scatterers comprising the shell. Furthermore, the one-shell fit did not adequately reproduce the feature at r' = 1.6 Å in the Fourier transform of the EXAFS data (Figure 5).

An improved fit to the data was obtained by dividing the first coordination sphere into two shells of scatterers at 2.01 and 2.15 Å (fit 2, Table II) or by adding a low-Z scatterer at 2.5–2.6 Å (fit 3, Table II). The best results were achieved by modeling the EXAFS with three shells (fit 4, Table II). This fit with two N/O scatterers at 2.02 Å, three N/O scatterers at 2.15 Å, and one C/O scatterer at 2.58 Å had a residual of 6% and adequately reproduced the Fourier transform of the data (Figure 5).

The study accomplished at Daresbury provided an independent corroboration of this interpretation. The EXAFS

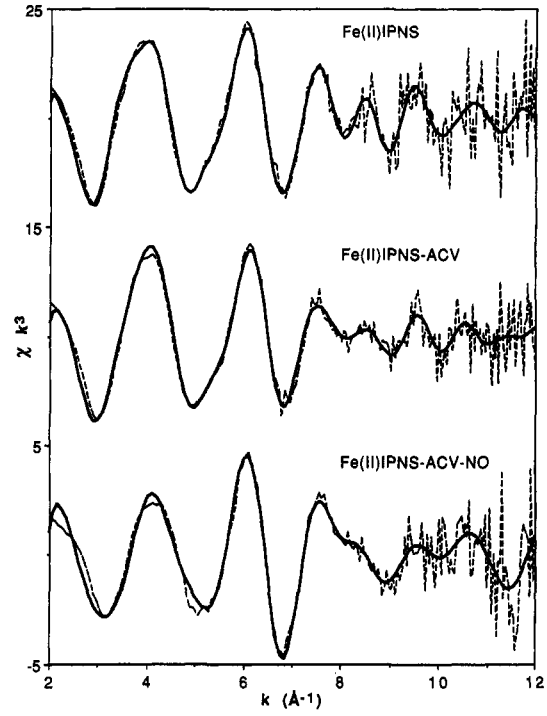

FIGURE 3: Fe K-edge EXAFS of IPNS samples (NSLS): data (k^3-weighted) (- - -) and multishell fits (—) of Fe(II)IPNS (top), Fe(II)IPNS–ACV (middle), and Fe(II)IPNS–ACV–NO (bottom).

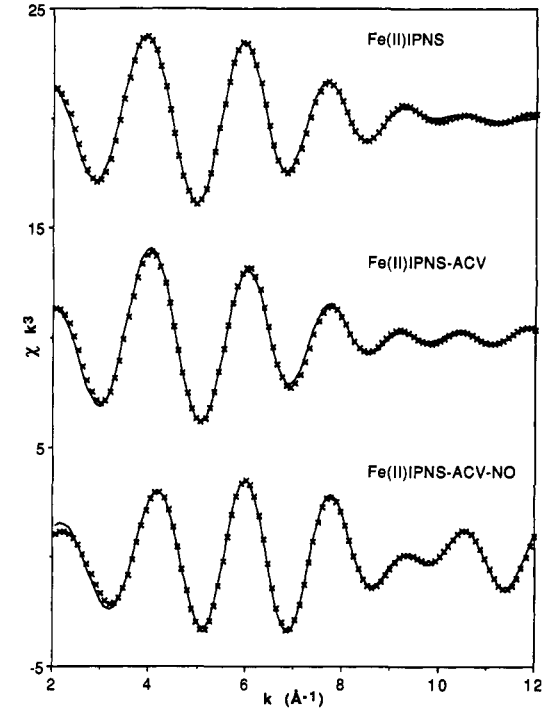

FIGURE 4: Fourier-filtered k^3-weighted EXAFS data (NSLS) (×) and first-coordination sphere fits using parameters from Table II (—) of Fe(II)IPNS (top), Fe(II)IPNS–ACV (middle), and Fe(II)-IPNS–ACV–NO (bottom). The backtransform ranges were 0.9–2.4, 0.8–2.4, and 0.8–2.3 Å, respectively.

Table II: Restricted Multishell Fits to EXAFS Data from Isopenicillin N Synthase Species

fit[a]	n	Fe–N/O	σ^2	n	Fe–N/O	σ^2	n	Fe–S	σ^2	n	Fe–O/C	σ^2	R_{FF}[b]
						Fe(II)IPNS							
1				5	2.09	0.0108							0.22
2	2	2.01	0.0009	3	2.15	0.0021							0.15
3				5	2.09	0.0112				1	2.54	0.0023	0.12
4	2	2.02	0.0022	3	2.15	0.0031				1	2.58	0.0040	0.06
						Fe(II)IPNS–ACV							
5				5	2.08	0.0100							0.31
6				5	2.09	0.0104				1	2.54	0.0011	0.17
7				4	2.07	0.0082	1	2.35	0.0050				0.08
						Fe(II)IPNS–ACV–NO							
8	1	1.71	0.0023	4	2.07	0.0087							0.58
9	1	1.71	0.0040	3	2.04	0.0048	1	2.33	0.0007				0.18
10	1	1.71	0.0041	3	2.04	0.0047	1	2.32	0.0004	1	2.61	0.0016	0.08

[a] Distances are in Å, Debye–Waller factors (σ^2) are in Å^2, and R_{FF} is the residual (RMS_{dev}/RMS_{dat}) between the fit and the Fourier-filtered data. [b] Backtransform ranges for Fe(II)IPNS, Fe(II)IPNS–ACV, and Fe(II)IPNS–ACV–NO are 0.9–2.4, 0.8–2.4, and 0.8–2.3 Å, respectively.

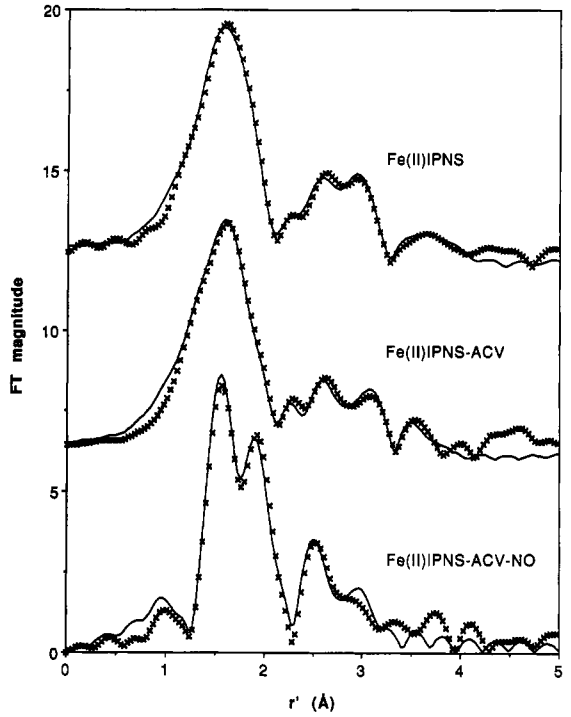

FIGURE 5: Fourier transforms of EXAFS data (NSLS) from Figure 3 (×) and multishell fits (—) of Fe(II)IPNS (top), Fe(II)IPNS–ACV (middle), and Fe(II)IPNS–ACV–NO (bottom). The Fourier transform ranges were 2.0–12.0, 2.0–14.0, and 2.0–14.0 Å^{-1}, respectively.

data and the Fourier transform, together with the Fourier-filtered data, are shown in Figure 6, and the parameters used in the final fit are summarized in Table III. The longer data range ($2.5 \leq k \leq 15$ Å^{-1}) obtained in this study allows a clearer assessment of the various backscattering contributions. This is especially true for the the inner coordination sphere, as is evident from the Fourier transform. Thus, the two shells at 2.01 and 2.15 Å are clearly resolved. The analysis of the EXAFS makes no clear distinction between an occupation number of 2 *vs* 3, or nitrogen *vs* oxygen atoms, in these two shells. However, the agreement between the simulated and experimental data is improved if 3, rather than 2, atoms are included in the first shell. The Daresbury data show clear evidence for a light atom at *ca.* 2.7 Å, which corresponds to the *ca.* 2.6 Å scatterer found in the NSLS data.

The first coordination sphere of Fe(II)IPNS–ACV [the enzyme–substrate complex of Fe(II)IPNS] could not be modeled adequately with one shell of nitrogen/oxygen scatterers. A fit with five Fe–N/O interactions at 2.08 Å had a

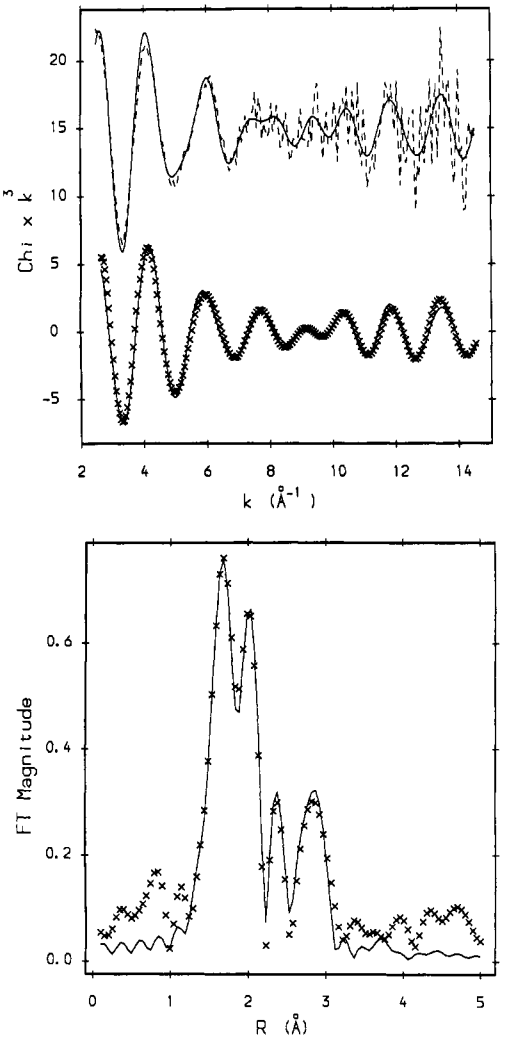

FIGURE 6: Fe K-edge EXAFS of Fe(II)IPNS (Daresbury). (a, top) Data (k^3-weighted) (- - -) and simulation using the parameters of Table III (—); Fourier-filtered (backtransform range 0.9–2.4 Å) EXAFS (k^3-weighted) (×) and simulation (—) using the first three coordination shells of Table III. (b, bottom) Fourier transform of the unfiltered EXAFS data (×) and simulation using the parameters of Table III (—).

Debye–Waller factor of 0.010 Å^2 and a residual of 31% (fit 5, Table II) and did not model the Fourier transform of the data well. Marked improvement was achieved by adding an Fe–O/C interaction at 2.54 Å (fit 6, Table II), as was seen with Fe(II)IPNS. The residual dropped to 17%, but the

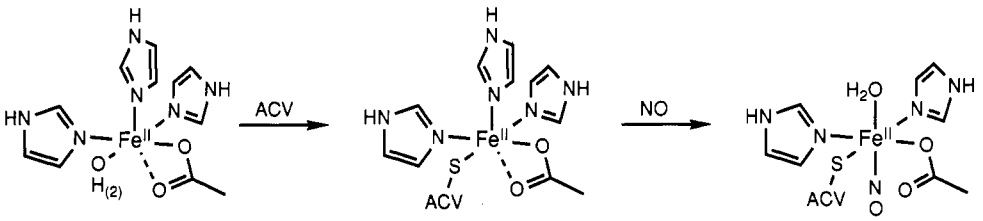

FIGURE 7: Proposed iron site coordination of Fe(II)IPNS, Fe(II)IPNS–ACV, and Fe(II)IPNS–ACV–NO.

Table III: Interpretation[a] of Daresbury EXAFS Data Recorded for Fe(II)IPNS

N	atom	r/Å	σ^2/Å^2
3	O/N	2.01	0.004
3	O/N	2.15	0.007
1	O	2.73	0.001
3	C	2.96	0.003
3	C	3.09	0.005
3	N	3.92	0.056
3	N	4.24	0.054

[a] Estimated uncertainties: $N \pm 1$; r ● 0.03 Å. No clear distinction is possible between backscattering from C, N, or O atoms; the particular assignments in the table are suggested as being chemically reasonable or, in the case of the outermost shell, for simplicity.

Debye–Waller factor of the 2.1 Å shell remained high (0.010 Å^2).

Inclusion of a sulfur atom at 2.3–2.4 Å resulted in a large reduction of the residual. A fit with four Fe–N/O at 2.07 Å and one Fe–S at 2.35 Å had a residual of 8% (fit 7, Table II) and modeled the Fourier-filtered and Fourier-transformed data well (Figures 4 and 5). Though the Debye–Waller factor of the shell at 2.07 Å was still somewhat high (0.008 Å^2), attempts to divide this shell into two with either one scatterer at ~2.0 Å and three at ~2.1 Å or two scatterers each at 2.0 and 2.1 Å gave only a slight improvement in the residual (7%). Furthermore, in both cases the Debye–Waller factor of the shell at 2.0 Å was too high (0.006 Å^2 for one scatterer and 0.018 Å^2 for two scatterers). The inclusion of a low-Z scatterer at 2.5–2.6 Å did not significantly improve the fit (residual of 7%) and resulted in a very large Debye–Waller factor for this scatterer (0.03 Å^2); therefore, the contribution of this last shell is not significant in the enzyme–substrate complex.

For the enzyme–substrate–nitric oxide complex [Fe(II)IPNS–ACV–NO], even a two-shell model was inadequate to reproduce the EXAFS. A fit with one Fe–N interaction at 1.71 Å and four Fe–N/O interactions at 2.07 Å had a residual of 58% (fit 8, Table II). A satisfactory fit for the E–S–NO complex was found only by incorporating an Fe–S interaction at 2.33 Å together with one Fe–N at 1.71 Å and three Fe–N/O at 2.04 Å to afford a residual of 18% (fit 9, Table II). The Debye–Waller factor of the sulfur atom was low (7×10^{-4} Å^2), similar to that found for the Fe–S interaction in the model complex [(TPA)Fe(S-2,4,6-$Me_3C_6H_2$)](ClO_4), which was 0.001 Å^2 (Table I). The addition of an Fe–O/C interaction at ~2.6 Å further improved the fit. The best fit found had one Fe–N at 1.71 Å, three Fe–N/O at 2.04 Å, one Fe–S at 2.32 Å, and one Fe–O/C at 2.61 Å, with a residual of 8% (fit 10, Table II). This fit reproduced the features of the Fourier-filtered and Fourier-transformed data well (Figures 4 and 5).

The backscattering contributions from the outer coordination spheres observed in the NSLS data for all three IPNS species were modeled similarly. For Fe(II)IPNS, the outer shells were fit with 3.5 Fe–C at 3.09 Å, 2.5 N/C at 3.44 Å, and 2.5 C at 4.18 Å. For Fe(II)IPNS–ACV, they were fit with 2.8 C at 3.07 Å, 2.2 N/C at 3.46 Å, and 2.4 C at 4.07 Å. For Fe(II)IPNS–ACV–NO, they were fit with 5 C at 3.07 Å and 3 N/C at 3.48 Å; no Fe–C interaction at 4.1–4.2 Å was used, as the model would have been overparametrized. However, addition of the outer coordination spheres gave no significant improvement to the models for the three IPNS species. Simulations of the outer coordination spheres of the Daresbury data for the Fe(II)IPNS center (Table III) included C atoms at 2.96 and 3.09 Å. However, the C_γ and N_γ atoms are not significant in the Fourier transform at *ca.* 4 Å (Figure 6), and these backscattering contributions were included in the simulation with unusually high Debye–Waller factors (Table III). Further investigations are necessary to clarify the backscattering contributions from the outer shells of the histidine imidazole groups.

DISCUSSION

We have analyzed the X-ray absorption spectra recorded for Fe(II)IPNS, its ACV complex, and its complex with ACV and NO; their implications are summarized by the scheme in Figure 7. For Fe(II)IPNS, our analysis supports conclusions derived from other spectroscopic studies (Chen *et al.*, 1989a,b; Ming *et al.*, 1990, 1991). Thus, in the holoenzyme we propose that the 2.15-Å scatterers are associated with the three nitrogens from coordinated histidine residues. These distances correspond well to those observed for Fe(II)–$N_{aromatic}$ bonds (Kitajima *et al.*, 1990; Ménage *et al.*, 1990); furthermore, the presence of three histidine ligands is also indicated by ^{1}H NMR studies (Ming *et al.*, 1990).

The Fe–O/C interaction at approximately 2.6–2.7 Å is required in the best fits of the data collected at both NSLS and Daresbury (fit 4, Table II; Table III); adding such an interaction was the only way to effectively model the beat pattern observed in the EXAFS data (Figures 3, 4, and 6) above $k = 7$ Å^{-1}, where the EXAFS waves reverse phase. This distance can be associated with the presence of a chelated carboxylate ligand. For example, the carboxylate carbons in (HB(^{i}Pr$_2$pz)$_3$)Fe(OAc)[2] and (HB(^{i}Pr$_2$pz)$_3$)Fe(OBz)(MeCN) (Kitajima *et al.*, 1990) are found at 2.48 and 2.52 Å from the iron center, respectively, while the more distant oxygen of the asymmetrically chelated benzoate in [Fe_2(DBE)$_2$(OBz)$_2$](ClO_4)$_2$ is found at 2.89 Å (Ménage & Que, 1990). The presence of a carboxylate has also been suggested from ^{1}H NMR spectra (Ming *et al.*, 1991).

The 2.01-Å shell must include one Fe–$O_{carboxylate}$ scatterer. The two Fe–$O_{carboxylate}$ bonds in [(HB(^{i}Pr$_2$pz)$_3$)Fe(OAc)] are 2.06 and 2.23 Å long,[2] while those in [Fe(TLA)OBz](BPh_4) are 2.04 and 2.30 Å long (Zang *et al.*, 1993). The other carboxylate oxygen at a longer distance either corresponds to the scatterer at 2.6–2.7 Å or does not significantly contribute to the EXAFS, as is found in the case of (HB(^{i}Pr$_2$pz)$_3$)Fe(OBz) (*vide supra*). The remaining scatterer at 2.01 Å is likely to arise from a bound solvent. Given its short bond length, we suggest that the solvent is present as hydroxide (Chaudhuri *et al.*, 1985), which could serve as the base that

accepts the cysteine thiol proton when ACV binds to Fe(II)IPNS.

The EXAFS data that we have recorded for Fe(II)IPNS both at NSLS and at Daresbury show some differences from those reported by Scott *et al.* (1992). While it was possible to model the active site of Fe(II)IPNS with one shell of five or six nitrogen/oxygen scatterers, as was found by Scott and co-workers, better fits were obtained when the first coordination sphere was divided into two shells of scatterers. These two shells are resolved in the Fourier-transformed spectrum of the Daresbury data because of its higher resolution (Figure 6). Furthermore, our data require the presence of a low-Z scatterer at approximately 2.6–2.7 Å, which we associate with a carboxylate ligand. As indicated above, the results of our EXAFS studies are consistent with other spectroscopic studies of native IPNS and structural studies of relevant iron(II) complexes.

For the Fe(II)IPNS–ACV complex, our data are best fit by a combination of four N/O scatterers at 2.07 Å and one S scatterer at 2.35 Å, in reasonable agreement with the results of Scott *et al.* (1992). The 2.07-Å shell is now comprised of all four endogenous ligands associated with Fe(II)IPNS, consistent with the analysis of ^{1}H NMR spectra indicating the presence of three histidine ligands and one carboxylate ligand (Ming *et al.*, 1991). The somewhat large Debye–Waller factor associated with this shell (σ^2 = 0.008 Å^2) suggests the presence of a broad range of distances, but splitting this shell into two does not significantly improve the residual.

The Fe–S interaction at 2.35 Å is consistent with the coordination of cysteinyl sulfur from ACV to the iron center. The Fe–S distance found is in excellent agreement with the 2.34-Å value observed for [Fe(TPA)(S-2,4,6-$Me_3C_6H_2$)]-(ClO_4). Its inclusion in the EXAFS fit corroborates earlier ^{57}Fe Mössbauer data. The addition of ACV to ^{57}Fe-enriched Fe(II)IPNS causes a decrease in the isomer shift value of the active site iron atom, which is consistent with the covalent binding of a thiolate moiety (Chen *et al.*, 1989a,b). Though EXAFS analysis cannot distinguish between an ACV sulfur atom and one from an endogenous cysteine residue, mutagenesis studies by Orville *et al.* (1992) have excluded the endogenous cysteines as ligands to the metal center. From the ^{57}Fe Mössbauer results and the effect of the addition of ACV on the EXAFS and XANES spectra (the low energy "tail" of the absorption edge, *vide supra*) of Fe(II)IPNS, it is likely that ACV binds to the iron(II) active site by its cysteinyl thiolate functionality.

However, the relatively large Debye–Waller factor of the sulfur atom at 2.35 Å (σ^2 = 0.005 Å^2, similar to that observed by Scott *et al.*) deserves further comment, as it is much larger than that of the Fe–S interaction in [(TPA)Fe(S-2,4,6-$Me_3C_6H_2$)](ClO_4) (0.001 Å^2). ACV does not bind strongly to Fe(II)IPNS (Chen *et al.*, 1989a; Ming *et al.*, 1991), and K_d was estimated by ^{57}Fe Mössbauer spectroscopy to be 18 mM for the dissociation of ACV from Fe(II)IPNS–ACV (Orville *et al.*, 1992). The large σ^2 value may reflect some dynamic disorder at the iron active site due to this weak binding interaction.

Our EXAFS results for the Fe(II)IPNS–ACV complex provide evidence for five ligands to the metal center. Neither the EXAFS analysis nor the pre-edge data allow us to make an unambiguous determination of the coordination number. As in the cases of [(TPA)Fe(S-2,4,6-$Me_3C_6H_2$)](ClO_4) and [(TMPzA)(Fe)(NO)Cl](BPh_4), a ligand with a bond length similar to the Fe–S bond length would be difficult to observe. A ligand with a long bond length may be associated with a bound water derived from proton transfer from the ACV thiol to the bound hydroxide in Fe(II)IPNS upon substrate binding or the more distant oxygen of an unsymmetrically chelated carboxylate (Figure 7). Both alternatives afford a readily displaceable ligand and would be poised to bind O_2 in the next step of the reaction mechanism.

The best fit found for Fe(II)IPNS–ACV–NO consists of one N at 1.71 Å, three N/O at 2.04 Å, one S at 2.32 Å, and one C/O at 2.61 Å. The short Fe–N distance is assigned to the NO ligand, as similarly short Fe–N distances are observed for [(TMPzA)Fe(NO)(Cl)](BPh_4) and other synthetic Fe–NO complexes (Enemark *et al.*, 1977; Haller *et al.*, 1979). The coordination of NO is also consistent with the much stronger intensity of the pre-edge feature.

It is tempting to associate the scatterer at 2.61 Å with the nitrosyl oxygen, but this assignment is unlikely. The Fe–$O_{nitrosyl}$ distance is not likely to be as short as 2.6 Å, and we see no such interaction in [(TMPzA)Fe(NO)(Cl)](BPh_4). The model compound has Fe–N_{NO} and N–O distances of 1.735 and 1.15 Å, respectively, typical of iron(II)–nitrosyl complexes, and an Fe–N–O angle of 157.1°, giving an Fe–O_{NO} distance of 2.83 Å. In all structurally characterized high-spin ($S = {}^3/_2$) iron(II)–nitrosyl species, the Fe–N–O angle is at least 147° and is usually greater than 155° (Enemark *et al.*, 1977; Haller *et al.*, 1979). As Fe(II)IPNS–ACV–NO is a high-spin complex (Chen *et al.*, 1989a) and our EXAFS results show that the nitrosyl nitrogen atom is 1.71 Å from the iron center, the nitrosyl oxygen atom must be at least 2.7 Å from the iron center. As with Fe(II)IPNS, we assign the interaction at 2.61 Å to a carboxylate ligand.

The Fe–S interaction at 2.32 Å was essential to reproduce the EXAFS data of Fe(II)IPNS–ACV–NO and its Fourier transform (Figures 4 and 5). Our observations corroborate the earlier notion that the ACV thiolate binds to the Fe–NO center, on the basis of the novel pink color exhibited by the Fe(II)IPNS–ACV–NO complex [compared to the olive green color found for other Fe(II)IPNS–NO complexes] (Chen *et al.*, 1989a). We note that the Debye–Waller factor of the sulfur scatterer has significantly decreased from that found in the Fe(II)IPNS–ACV complex. The low σ^2 value for the NO complex (4×10^{-4} Å^2) is comparable to that found for [(TPA)Fe(S-2,4,6-$Me_3C_6H_2$)](ClO_4) (1×10^{-3} Å^2) and consistent with the observation that ACV binds more tightly to Fe(II)IPNS in the presence of NO (Chen *et al.*, 1989a).

The remaining ligands are associated with the 2.04-Å distance. This distance is somewhat short to be ascribed only to histidine ligation, even taking the more "ferric" character of the Fe–NO center into consideration, as Fe(III)–$N_{aromatic}$ distances are similar to those found for iron(II), *ca.* 2.1 Å (Armstrong & Lippard, 1984; Armstrong *et al.*, 1984; Ménage & Que, 1990). Since a carboxylate is implicated by the 2.61-Å interaction, an Fe–$O_{carboxylate}$ interaction at ~2.0 Å would be reasonable (Carrell *et al.*, 1988). So a combination of two histidines and one carboxylate could give rise to the 2.04-Å shell.

These inferences derived from the EXAFS analysis of Fe(II)IPNS–ACV–NO must be reconciled with those derived from ^{1}H NMR data, which show the loss of paramagnetically shifted signals due to one histidine and the carboxylate relative to Fe(II)IPNS and Fe(II)IPNS–ACV (Ming *et al.*, 1991), and EPR and UV–vis data which suggest the presence of three exogenous ligands: NO, ACV, and solvent (Chen *et al.*, 1989b). Taking the various spectroscopic studies into account, we propose that NO binding to Fe(II)IPNS–ACV results in the displacement of a histidine ligand and the introduction of

a solvent molecule, affording an Fe(II)–NO center that is also ligated by solvent, two histidine imidazoles, a cysteine thiolate from ACV, and one carboxylate (Figure 7). The EXAFS analysis argues against the dissociation of the carboxylate ligand. The disappearance of the carboxylate resonances from the ^{1}H NMR spectrum may indicate a change in conformation that either brings the CH_2 protons closer to the metal center, thereby broadening these resonances, or results in smaller paramagnetic shifts for the carboxylate protons.

In conclusion, our EXAFS analysis builds on the earlier results of Scott *et al.* (1992) and provides evidence for an iron coordination environment consisting of three histidines and a carboxylate in native isopenicillin N synthase, in agreement with earlier NMR studies (Ming *et al.*, 1991). The three His, one RCO_2^- ligand environment has also been found in the active sites of iron superoxide dismutase (Stallings *et al.*, 1983; Stoddard *et al.*, 1990) and soybean lipoxygenase[3] (Boyington *et al.*, 1993) and may represent a common structural motif among mononuclear non-heme iron-containing enzymes. Indeed, IPNS from *C. acremonium* contains a D131-E132xxH135 sequence (Samson *et al.*, 1985) analogous to the D156xxxH160 sequence found in iron superoxide dismutase (Carlioz *et al.*, 1988). The aspartate and histidine are two of the iron ligands in iron superoxide dismutase; the aspartate or glutamate and the histidine in the former sequence may have similar roles in the IPNS active site. The ACV sulfur atom coordinates to the iron center in both the enzyme–substrate and enzyme–substrate–nitric oxide complexes at a distance of ~2.3 Å, a value typical of Fe(II)–SR bonds. The structural information derived from this study (Figure 7) confirms features of the proposed mechanism for IPNS action (Baldwin *et al.*, 1992) and provides a foundation for further insights into the bioinorganic chemistry of this fascinating enzyme.

ACKNOWLEDGMENT

We thank Dr. Li-June Ming for the preparation and characterization of protein samples and Drs. Richard Holz and Timothy Elgren for assistance with data collection. We acknowledge the generosity of Professor Nobumasa Kitajima for a sample of [Fe(HB(^{i}Pr$_2$pz)$_3$)OBz] and for providing the crystallographic results on [Fe(HB(^{i}Pr$_2$pz)$_3$)OAc] prior to publication. We especially appreciate the assistance of Dr. Syed Khalid of the Biostructures Institute at beamline X9 of the NSLS and the operators at CHESS.

SUPPLEMENTARY MATERIAL AVAILABLE

Figures of EXAFS data and multishell fits of model complexes for IPNS species and tables of complete multishell fits to data from model complexes and IPNS species (5 pages). Ordering information is given on any current masthead page.

REFERENCES

Armstrong, W. H., & Lippard, S. J. (1984) *J. Am. Chem. Soc. 106*, 4632–4633.

Armstrong, W. H., Spool, A., Papaefthymiou, G. C., Frankel, R. B., & Lippard, S. J. (1984) *J. Am. Chem. Soc. 106*, 3653–3667.

Baldwin, J. E. (1989) in *Recent Advances in the Chemistry of β-Lactam Antibiotics* (Bentley, P. H., & Southgate, R., Eds.) Chapter 1, Royal Society of Chemistry, London.

Baldwin, J. E., & Abraham, E. P. (1988) *Nat. Prod. Rep. 5*, 129–145.

Baldwin, J. E., & Bradley, M. (1990) *Chem. Rev. 90*, 1079–1088.

Baldwin, J. E., Blackburn, J. M., Schofield, C. J., & Sutherland, J. D. (1990) *FEMS Microbiol. Lett. 68*, 45–52.

Baldwin, J. E., Lynch, G. P., & Schofield, C. J. (1992) *Tetrahedron 48*, 9085–9100.

Binsted, N., Campbell, J. W., Gurman, S. J., & Stephenson, P. C. (1991) *SERC Daresbury Laboratory EXCURV92 Program* (computer code for calculating the Hedin–Lundqvist potentials was provided by Prof. J. J. Rehr of the University of Washington, Seattle).

Boyington, J. C., Gaffney, B. J., & Amzel, L. M. (1993) *Biophys. J. 64*, A349.

Bunker, G. B., & Stern, E. A. (1984) *Phys. Rev. Lett. 52*, 1990–1993.

Carlioz, A., Ludwig, M. L., Stallings, W. C., Fee, J. A., Steinman, H. M., & Touati, D. (1988) *J. Biol. Chem. 263*, 1555–1562.

Carrell, C. J., Carrell, H. L., Erlebacher, J., & Glusker, J. P. (1988) *J. Am. Chem. Soc. 110*, 8651–8656.

Chaudhuri, P., Wieghardt, K., Nuber, B., & Weiss, J. (1985) *Angew. Chem., Int. Ed. Engl. 24*, 778–779.

Chen, V. J., Orville, A. M., Harpel, M. R., Frolik, C. A., Surerus, K. K., Münck, E., & Lipscomb, J. D. (1989a) *J. Biol. Chem. 264*, 21677–21681.

Chen, V. J., Frolik, C. A., Samson, S., Gesellchen, P. D., Orville, A. M., Harpel, M. R., Lipscomb, J. D., Surerus, K. K., & Münck, E. (1989b) *J. Inorg. Biochem. 36*, H052.

Enemark, J. H., Feltham, R. D., Huie, B. T., Johnson, P. L., & Swedo, K. B. (1977) *J. Am. Chem. Soc. 99*, 3285–3292.

Garner, C. D., & Feiters, M. C. (1987) in *Biophysics and Synchrotron Radiation* (Bianconi, A., & Congiu Castellano, A., Eds.) pp 136–146, Springer-Verlag, Berlin.

Gurman, S. J., Binsted, N., & Ross, I. (1984) *J. Phys. C 17*, 143–151.

Gurman, S. J., Binsted, N., & Ross, I. (1986) *J. Phys. C 19*, 1845–1861.

Haller, K. J., Johnson, P. L., Feltham, R. D., & Enemark, J. H. (1979) *Inorg. Chim. Acta 33*, 119–130.

Hedin, L., & Lundqvist, S. (1969) *Solid State Phys. 23*, 1–181.

Jiang, F., Peisach, J., Ming, L.-J., Que, L., Jr., & Chen, V. J. (1991) *Biochemistry 30*, 11437–11445.

Kitajima, N., Fukui, H., Moro-oka, Y., Mizutani, Y., & Kitagawa, T. (1990) *J. Am. Chem. Soc. 112*, 6402–6403.

Kriauciunas, A., Frolik, C. A., Hasell, T. C., Skatrud, P. L., Johnson, M. G., Holbrook, N. L., & Chen, V. J. (1991) *J. Biol. Chem. 266*, 11779–11788.

Lee, P. A., & Pendry, J. B. (1975) *Phys. Rev. B 11*, 2795–2811.

McKale, A. G., Veal, B. W., Paulikas, A. P., Chan, S.-K., & Knapp, G. S. (1988) *J. Am. Chem. Soc. 110*, 3763–3768.

Ménage, S., & Que, L., Jr. (1990) *Inorg. Chem. 29*, 4293–4297.

Ménage, S., Brennan, B. A., Juarez-Garcia, C., Münck, E., & Que, L., Jr. (1990) *J. Am. Chem. Soc. 112*, 6423–6425.

Ming, L.-J., Que, L., Jr., Kriauciunas, A., Frolik, C. A., & Chen, V. J. (1990) *Inorg. Chem. 29*, 1111–1112.

Ming, L.-J., Que, L., Jr., Kriauciunas, A., Frolik, C. A., & Chen, V. J. (1991) *Biochemistry 30*, 11653–11659.

Müller, J. E., & Schaich, W. L. (1983) *Phys. Rev. B 27*, 6489–6492.

Orville, A. M., Chen, V. J., Kriauciunas, A., Harpel, M. R., Fox, B. G., Münck, E., & Lipscomb, J. D. (1992) *Biochemistry 31*, 4602–4612.

Que, L., Jr. (1989) in *Iron Carriers and Iron Proteins* (Loehr, T. M., Ed.) Chapter 6, VCH, New York.

Robinson, J. A. (1988) *Chem. Soc. Rev. 17*, 383–452.

Roe, A. L., Schneider, D. J., Mayer, R. J., Pyrz, J. W., & Que, L., Jr. (1984) *J. Am. Chem. Soc. 106*, 1676–1681.

Samson, S. M., Belagaje, R., Blankenship, D. T., Chapman, J. L., Perry, D., Skatrud, P. L., Van Frank, R. M., Abraham, E.

[3] B. J. Gaffney, personal communication.

P., Baldwin, J. E., Queener, S. W., & Ingolia, T. D. (1985) *Nature (London) 318*, 191–194.
Scarrow, R. C., Maroney, M. J., Palmer, S. M., Que, L., Jr., Roe, A. L., Salowe, S. P., & Stubbe, J. (1987) *J. Am. Chem. Soc. 109*, 7857–7864.
Scott, R. A. (1985) *Methods Enzymol. 11*, 414–459.
Scott, R. A., Wang, S., Eidsness, M. K., Kriauciunas, A., Frolik, C. A., & Chen, V. J. (1992) *Biochemistry 31*, 4596–4601.
Shulman, R. G., Yafet, Y., Eisenberger, P., & Blumberg, W. E. (1976) *Proc. Natl. Acad. Sci. U.S.A. 73*, 1384–1388.
Stallings, W. C., Powers, T. B., Pattridge, K. A., Fee, J. A., & Ludwig, M. L. (1983) *Proc. Natl. Acad. Sci. U.S.A. 80*, 3879–3883.
Stern, E. A., & Heald, S. M. (1979) *Rev. Sci. Instrum. 50*, 1579–1582.
Stoddard, B. L., Howell, P. L., Ringe, D., & Petsko, G. A. (1990) *Biochemistry 29*, 8885–8893.
Teo, B.-K. (1981) in *EXAFS Spectroscopy, Techniques and Applications* (Teo, B.-K., & Joy, D. C., Eds.) pp 13–58, Plenum, New York.
Teo, B.-K., & Lee, P. A. (1979) *J. Am. Chem. Soc. 101*, 2815–2832.
Teo, B.-K., Antonio, M. R., & Averill, B. A. (1983) *J. Am. Chem. Soc. 105*, 3751–3762.
Zang, Y., Elgren, T. E., Dong, Y., & Que, L., Jr. (1993) *J. Am. Chem. Soc. 115*, 811–813.
Zhang, Y., Pavlosky, M. A., Brown, C. A., Westre, T. E., Hedman, B., Hodgson, K. O., & Solomon, E. I. (1992) *J. Am. Chem. Soc. 114*, 9189–9191.